Chemical Science

ROYAL SOCIETY OF CHEMISTRY

EDGE ARTICLE

View Article Online
View Journal | View Issue

Cite this: *Chem. Sci.*, 2024, **15**, 14202

All publication charges for this article have been paid for by the Royal Society of Chemistry

Low thermal quenching of metal halide-based metal–organic framework phosphor for light-emitting diodes†

Xiao-Gang Yang, * Ying-Jun Chen, Pei-Pei Yin, Yan Li, Shu-Yao Yang, Yi-Man Li and Lu-Fang Ma *

Phosphor-converted white light-emitting diodes (PC-WLEDs) have attracted considerable attention in solid-state lighting and display. However, urgent issues of thermal quenching and high cost remain formidable challenges. Herein, a novel metal–organic framework (MOF) phosphor [$CdCl_2$(AD)] was facilely prepared using a mixture of $CdCl_2$ and acridine (AD) under solvothermal conditions. It shows intensive green emission with a long lifetime of 31.88 ns and quantum yield of 65% while maintaining 95% and 84% of its initial emission intensity after remaining immersed in water for 60 days and being heated to 150 °C, respectively. The low thermal quenching of this MOF material is comparable to or can even exceed that of commercial inorganic phosphors. The combination of experiments and theoretical calculations reveals that the alternating arrangement of delocalized AD π-conjugated systems and $CdCl_2$ inorganic chains through strong coordination bonds and π···π stacking interactions imparts the MOF phosphor with high thermal stability and optoelectronic performance. The successful fabrication of green and white LED devices by coating [$CdCl_2$(AD)] and/or N630 red phosphor on a 365/460 nm commercial diode chip suggests a promising and potential alternative to commercial phosphors.

Received 26th June 2024
Accepted 31st July 2024

DOI: 10.1039/d4sc04228j

rsc.li/chemical-science

Introduction

Phosphor-converted white light-emitting diodes (PC-WLEDs) have attracted great attention in the fields of solid-state lighting owing to their high luminescence efficiency and long lifetime characteristics.[1–7] The pre-coating of yellow or multiple colored (blue, green, and red) phosphors onto blue or ultraviolet diode chips are two mainstream methods for preparing PC-WLEDs.[8] However, the heat generated during the high drive current applied to the inner diode chips causes a universal thermal quenching (TQ) effect which can decrease the luminescent performance of phosphors.[9–12] Therefore, the minimization of TQ for phosphors is an urgent problem for their applications in WLEDs. Even though breakthrough progresses have been made in zero-thermal quenching inorganic phosphors due to their rigid structures,[12–14] high-cost (containing certain expensive elements) and complicated preparation methods (about 1000 °C high-temperature sintering process) hinder the development of inorganic materials.[2] It is still a huge challenge to develop new types of phosphors with low cost and low TQ.

Metal–organic frameworks (MOFs) are a new type of organic–inorganic hybrid materials constructed by metal cations/clusters and organic ligands through strong coordination bonds. Benefiting from their advantages, such as facile synthesis routes, easy functionalization, excellent structural stability and diversity, MOFs have been applied in numerous areas, including catalysis, photoelectric devices, bioimaging, nonlinear optics, and so on.[15–23] As a subclass of MOFs, luminescent MOFs have been proven to be futuristic phosphor materials for PC-WLEDs technology owing to their excellent optical properties, tunable energy levels, and wide range of emission colors.[2] Despite promising results that were recently achieved on MOF-based phosphors for PC-WLEDs with high luminescent efficiency,[24,25] emission losses induced by lower thermal stability still need to be addressed.

It has been demonstrated that the structural rigidity due to the strong coordination bonds and bulky steric hindrance near the metal ions can greatly enhance the stability of MOFs.[26–28] Following this proposition, a suitable selection of photoactive organic ligands with various coordination numbers is indispensable to construct MOFs with dramatic geometric frameworks and excellent luminescent properties.[29–32] The heterocyclic compound, acridine (AD), is an outstanding chromophore, which plays an important role in molecular luminescent and optoelectronic materials. The larger π-conjugated

College of Chemistry and Chemical Engineering, Luoyang Normal University, Henan Province Function-Oriented Porous Materials Key Laboratory, Luoyang 471934, P. R. China. E-mail: yxg2233@126.com; mazhuxp@126.com

† Electronic supplementary information (ESI) available: Experimental details and structure data table, PXRD, TGA and photoluminescent spectra. CCDC 2364270. For ESI and crystallographic data in CIF or other electronic format see DOI: https://doi.org/10.1039/d4sc04228j

system has an affinity to form denser π-stacking, leading to outstanding photophysical properties by the introduction of various organic and inorganic components.[33] Our recent work showed that the larger steric hindrance of AD cations arranged in dense stacking mode can afford effective organic water-resisting layers to maintain the long-term stability of organic–inorganic hybrid perovskite (OIHPs) in water.[34]

On the other hand, the selection of proper inorganic components is also a crucial factor. Among various metal ions/clusters, metal halides initially gained worldwide attention because of their unique crystallographic/electronic structures with isolated building units and fascinating optical characteristics.[35] Metal halides are typically used in the construction of OIHPs. As a type of emerging luminescent material, OIHPs have attracted unparalleled interest in the fields of photovoltaics, photodetectors, light-emitting diodes, and lasers.[36,37] However, physicochemical stability is still a critical issue in achieving their effective practical applications. Different from the weak electrostatic and hydrogen bond interactions in OIHPs, vigorous coordination bonds between organic chromophore ligands and metal halides would enable high thermal and water stability for MOF materials. In this study, a cadmium halide inorganic chains-based MOF [$CdCl_2$(AD)] (**1**) was synthesized through a facile solvothermal process. The AD organic chromophores are arranged into an infinite π-conjugated chain featuring dense H-aggregation in an orderly fashion, promoting the migration of charge carriers. The assembly of cadmium halide inorganic chains and AD π-conjugated system provides periodic distribution of electron donor and acceptor at the molecular level. These structural features endow the title MOF with high thermal and water stability, as well as photoelectric performance. It can maintain 84% of the initial emission intensity at 150 °C and exceed several commercial inorganic phosphors.

Results and discussion

Light-yellow block crystals (Fig. S1†) that were suitable for X-ray single-crystal detection were isolated under solvothermal conditions at 120 °C for 3 h. Powder X-ray diffraction (PXRD) measurements revealed that the main diffraction peaks of the as-prepared **1** match well with the simulated peaks from the single crystal diffraction data (Fig. S2†), suggesting the successful synthesis of the pure samples of the target complex. Single crystal X-ray diffraction analysis reveals that **1** crystallizes in a monoclinic system with the space group of $P2_1/c$ (Table S1†). In the structure of **1**, each asymmetric unit consists of one Cd(II) cation, one AD ligand, and two chlorine anions. All Cd(II) cations are five-coordinated by four chlorine anions and one nitrogen atom from the AD ligand, forming a distorted trigonal bipyramid geometry (Fig. S3†). The Cd(II) cations are connected by Cl anions to form an infinite 1D $CdCl_2$ inorganic chain along the *a*-direction. The AD ligands hang on both sides of the chain through the Cd–N bond (Fig. 1a).

Owing to the bulk π-conjugated AD molecules, adjacent chains are linked to form a 2D layer structure through π···π stacking interactions (with a centroid-to-centroid distance of

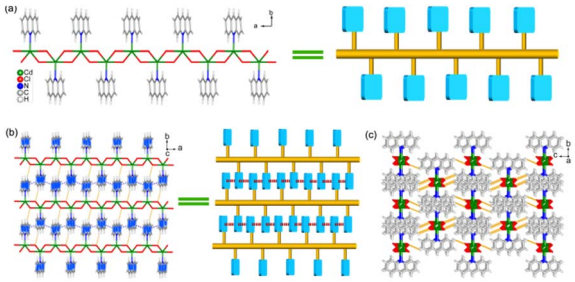

Fig. 1 (a) View of the 1D chain of **1** running along the *a*-direction. (b) View of the 2D network of **1** running along the *ab*-plane extended by π···π stacking and C–H···Cl interactions between adjacent chains. (c) 3D structure extended by C–H···Cl interactions between the 2D layers.

3.92 and 3.87 Å) between the AD molecules (Fig. 1b). The C–H···Cl hydrogen bonding interactions (H···Cl: 2.83 and 3.31 Å) further strengthen such a 2D layer, and further extend the layers to a 3D network (Fig. 1c). The view along the *a*-direction (Fig. S4†) demonstrates that the 3D structure displays an alternating arrangement of electronic acceptor in the $CdCl_2$ inorganic chains and AD π-conjugated system electronic donor, featuring special heterojunction at the molecular level. Based on the above structure analysis, it can be concluded that the AD organic chromophores are tightly anchored by the $CdCl_2$ inorganic chains and arranged in an infinite π-conjugated system, which helps afford delocalized π electrons for efficient charge transfer.

The photophysical properties of **1** were investigated in a solid state at room temperature. The solid-state UV-vis absorption spectrum of **1** shows a broad absorption peak with a band edge of about 490 nm (Fig. S5†). The excitation spectrum also features a broad region in the range of 300 to 470 nm. Upon excitation at 400 nm, **1** displays strong green emission at 504 nm (Fig. 2a). Correspondingly, crystals (Fig. 2 inset) and the powdered sample (Fig. S6†) of **1** emit intense green light

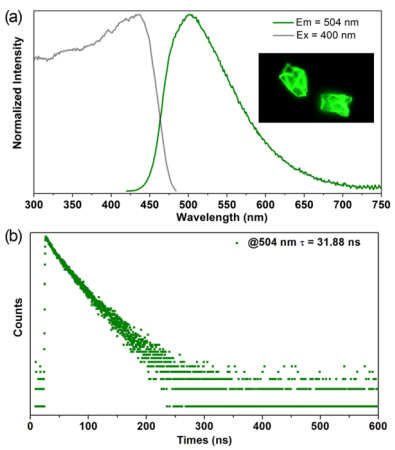

Fig. 2 Normalized excitation, emission spectra, (a) and photoluminescence decay curve (b) of **1** in solid state measured at room temperature. The inset shows crystals of **1** under UV light.

irradiated under the UV light (365 nm). The photoluminescence (PL) decay curve measured at room temperature gives a long lifetime of 31.88 ns (Fig. 2b). The single-exponential PL decay curve and long-lived emission reveal charge transfer characteristic of **1**.[38] In addition, the as-prepared **1** also features high PL quantum yield (PLQY) of 65%. Herein, both the emission lifetime and PLQY of **1** are longer and higher than the pristine AD, AD-based cocrystals,[33] and organic–inorganic hybrid perovskite.[34] The high PL performance of **1** can be attributed to the fact that it features more rigid surroundings induced by strong coordination bonds, π···π stacking, and hydrogen bond interactions, which can greatly limit molecular thermal vibration and non-radiative relaxation.

To obtain insights into the photophysical properties of **1**, the frontier molecular orbitals, band gap, and density of states (DOS) were investigated by the periodic density functional theory (DFT) calculations. Owing to the alternately spatial arrangement of inorganic and organic components, a complete separation of molecular orbitals is displayed between the highest occupied molecular orbitals (HOMOs) and the lowest unoccupied molecular orbitals (LUMOs). This phenomenon is in line with the AD-based cocrystal complex[33] and organic–inorganic hybrid perovskite.[34] However, the electron density of the HOMO in **1** is completely localized on the continuous AD π-conjugated system (Fig. 3a and S7a†), whereas the LUMO is exclusively distributed on the $CdCl_2$ inorganic chains (Fig. 3b and S7b†). The electron transition between the HOMO and the LUMO involves electron migration from the AD π-conjugated system to $CdCl_2$ inorganic chains. Meanwhile, it is worth noting that π-bonds between the AD molecules delocalized along the *a*-direction to generate a new type of π electronic channels (Fig. S7a†), which is in favor of charge separation and migration. By contrast, a reverse electron density distribution was found in organic–inorganic hybrid perovskite,[34] which caused the electron density to appear on the lead chloride inorganic layer in HOMO and the AD organic components in LUMO. The photophysical process in the cocrystal complexes shows electron transition from isophthalic acid derivatives to AD molecules.[33] The entire difference stems from the charge state of the AD compound. In **1**, the AD molecules are electroneutral (Fig. S7c†), whereas the protonated AD in the other two examples is electropositive, acting as an electron acceptor; the electronegative inorganic (lead chloride) or organic (isophthalic acid derivatives) conformers are electron donors. In spite of these differences, the title complex **1** has a HOMO and LUMO energy level of −5.900 and −3.482 eV, respectively. The HOMO–LUMO energy gap was calculated as 2.418 eV (Fig. 3c), which may correspond to the PL emission peak around 504 nm (2.460 eV). These values are close to those for the AD-IPA and AD-IPB cocrystal complexes.[33] The total/partial electronic density of states (TDOS/PDOS) analyses (Fig. 3d and S8†) reveal that the 2p orbitals of carbon atoms in AD, the 3p orbitals of chloride, and the 3d orbitals of cadmium in **1** contribute more to the generation and collection of photoexcitation electrons. Therefore, the molecular level heterojunction of **1** possesses completely separate frontier molecular orbitals between the organic donors and the inorganic acceptors. Such a special electronic structure endows both long lifetime and high PLQY for **1** due to long-term photoexcited electrons migrating from the delocalized AD π electronic channels to the electron-deficient $CdCl_2$ inorganic chains.

High thermal stability and low thermal quenching are critical criteria for phosphors applied in PC-WLEDs.[11] The thermogravimetric analysis (TGA) curve (Fig. S9†) indicates a weight loss of 49.7% at a heating range from 270 to 350 °C, which can be due to the loss of AD molecules (calculated value was 49.4%). The decomposition temperature of **1** is higher than the melting point of the pure AD (110 °C), implying highly enhanced thermal stability of the AD phosphor owing to strong coordination bonds, π···π stacking, and hydrogen bond interactions in the coordination polymer. Fig. S10† depicts the temperature-dependent PL spectra of **1**. It can be observed that the PL intensity shows a gradually increasing trend from ambient conditions (293 K) to 53 K accompanied by a distinct red-shift

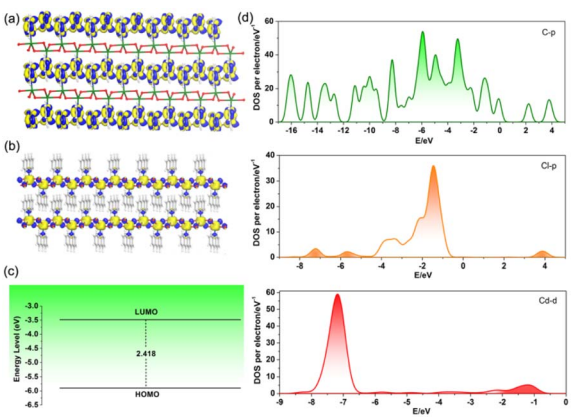

Fig. 3 View of the HOMO (a), LUMO (b), and relevant energy level/gap (c) for the DFT optimized structure of **1**. (d) Partial electronic density of states (PDOS) of **1**.

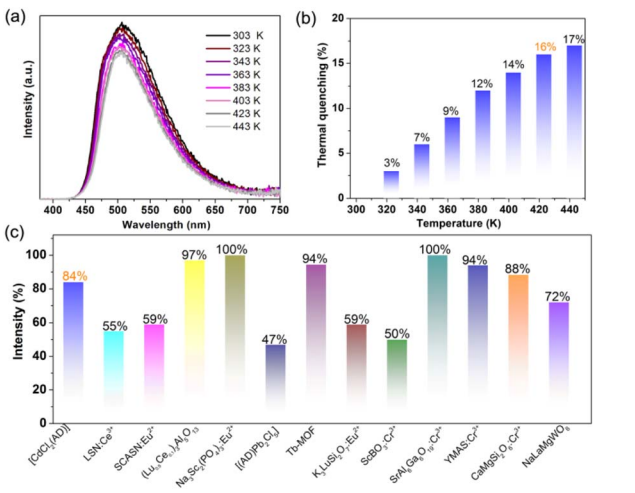

Fig. 4 PL spectra (a) and thermal quenching compared to 293 K (b) of **1** recorded in the temperature range of 303–443 K. (c) A comparison of emission intensity values at 423 K (150 °C) compared to room temperature for some developed phosphors.

from green to yellow emission (Fig. S11†). The function between maximum PL intensity and corresponding temperature in the range of 53–293 K was fitted as $y = 554x^{0.285}$ with an R^2 of 0.989 (Fig. S12†). Herein, the thermochromism of PL red-shift may arise from denser π-stacking of AD molecules under low temperatures. Upon further heating from 303 to 433 K, the emission peak was maintained at 504 nm without a change in emission color (Fig. 4a). Meanwhile, the maximum PL intensity only decreased by 16% of its initial emission intensity (Fig. 4b) after being heated to 423 K (the working temperature of LEDs can reach 150 °C at high drive current applied to the inner diode chips). Additional fatigue resistance results (Fig. S13†) show a reversible change in PL intensity repeated at least six times during heating–cooling cycles between 303 and 423 K. The above results further verify that the [$CdCl_2$(AD)] phosphor is highly resistant to thermal quenching, ensuring its practical applications. Fig. 4c and Table S3† list the thermal stability and photophysical properties of some developed phosphors. [$CdCl_2$(AD)] can maintain 84% of its initial emission intensity (compared to room temperature) at 423 K. This value is close to those of $(Lu_{0.9}Ce_{0.1})_3Al_5O_{13}$,[8] $Na_3Sc_2(PO_4)_3$:Eu^{2+},[13] Tb-MOF,[39] $SrAl_6Ga_6O_{19}$:Cr^{3+},[40] YMAS:Cr^{3+},[41] and $CaMgSi_2O_6$:Cr^{3+},[42] and exceeds the values for [(AD)Pb_2Cl_5],[34] $K_3LuSi_2O_7$:Eu^{2+},[43] $ScBO_3$:Cr^{3+},[44] $NaLaMgWO_6$,[45] as well as commercial phosphors LSN:Ce^{3+} and SCASN:Eu^{2+}.[8] The comparison revealed that the phosphor reported in this work, [$CdCl_2$(AD)], simultaneously possesses outstanding optical performance, low thermal quenching, and accessible synthesis. These merits enable it to be a promising candidate for solid-state lighting.

Its water stability was examined by immersing the sample in water for 60 days. The PXRD pattern of the recollected sample could match the simulated one (Fig. 5a), confirming that complex **1** maintains the crystal structure after remaining soaked in water for 60 days. The SEM image (Fig. 5b and S14†) shows negligible changes in morphology. The PL intensity of **1** retained 95% of the initial intensity after the same test time (Fig. 5c). Insets show the solid sample soaked in water and the recollected sample radiated under UV (365 nm) light, which exhibits intense green emission. The time-resolved PL measurement shows a slight decrease in the PL lifetime to 30.05 ns (Fig. 5d). The PLQY also maintains a high value of 63%. To date, achieving thermal and water stability is a thorny problem for organic–inorganic hybrid perovskite, although this material possesses excellent photoelectric properties. Most of the reported works focus on surface modification.[27–29] In our recent work, the introduction of organic cations with bulk π-conjugated planes can strongly inhibit the ingression of water molecules into the perovskite.[34] In this work, the direct coordination of AD and $CdCl_2$ inorganic chains provides a new strategy to enhance the stability of organic–inorganic hybrids. The dense π-stacking of AD molecules around $CdCl_2$ inorganic chains affords a compact organic water-resisting system to prevent corrosion from water molecules. Meanwhile, the tight anchor of the dense π-conjugated system by the $CdCl_2$ inorganic chains through strong coordination bonds further strengthens the rigid matrix with long-term stability.

As mentioned above, the π-conjugated chains of AD molecules delocalized to generate long-range order electron channels (Fig. 6a and 3a). These channels are in favor of affording more time for exciton hopping events, exhibiting high optoelectronic efficiency. To verify this point, the excited state activity of **1** was evaluated by photocatalytic degradation of dye methyl orange (MO) in a neutral aqueous solution under irradiation. The maximum absorbance of MO at 464 nm was detected to determine the decrease in the concentration of this organic dye. In comparison with the blank experiments, the presence of MOF photocatalyst can efficiently degrade 99.73%

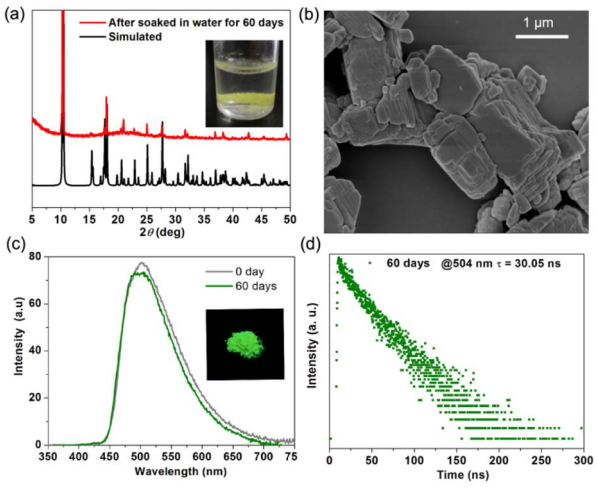

Fig. 5 PXRD pattern (a), SEM image (b), PL spectra (c), and time-resolved PL decay curve (d) of **1** after being soaked in water for 60 days. Insets show the solid sample soaked in water and recollected sample radiated under UV (365 nm) light.

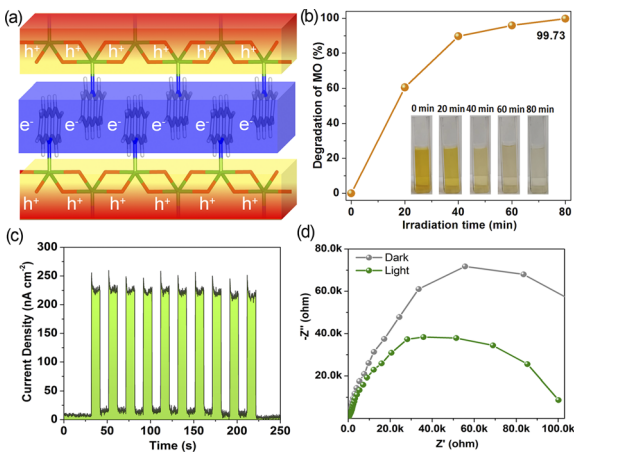

Fig. 6 (a) A schematic diagram of the arrangement of electrons and hole transport channels in **1**. (b) Percentage photocatalytic degradation of the methyl orange dye (20 mg L^{-1}) in the presence of powdered **1** (10 mg) in a neutral aqueous solution. Insets show the photos of MO aqueous solution after different illumination times. (c) Transient photocurrent measurements of **1** under repeated on/off cycles of illumination at 0 V *vs.* Ag/AgCl. (d) Electrochemical impedance spectroscopy Nyquist plots of the powder of **1** coated on ITO under dark and illumination conditions without additional bias potential.

of the MO dye within 80 min (Fig. 6b and S15†). The kinetics of photocatalytic dye degradation afforded the rate constant (k) of 0.0723 min^{-1} (Fig. S16†), according to the pseudo-first-order kinetic model of the Langmuir–Hinshelwood model: $\ln(C/C_0) = kt$, in which C_0 and C is the initial and time t concentration of MO. The measurements of transient photocurrent for the powder of **1** modified indium tin oxide (ITO) electrode show minimum/maximum current density of 6.3/259.6 nA cm^{-2} under dark/illumination conditions with on–off current ratio of 41, revealing efficient photo-induced charge separation efficiency of **1** (Fig. 6c). Nyquist plots for electrochemical impedance spectroscopy reveal that the charge transfer resistance of **1** under illumination is significantly lower than that under the dark conditions, suggesting the fastest charge transfer rate for the excited state of **1** (Fig. 6d). Furthermore, the study of the active species in the photocatalytic process of **1** suggest that the singlet oxygen ($^1O_2$) and hole (h^+) have significant roles for the MOF photocatalyst (Fig. S17†). High water stability also endows long reusability for the photocatalyst of **1**. It shows almost no obvious decrease in the photocatalytic degradation of MO after five repeated cycles (Fig. S18†). The elemental compositions and chemical states of **1** after photocatalytic degradation were further investigated by PXRD, SEM, and X-ray photoelectron spectroscopy (XPS). PXRD patterns (Fig. S19†) suggest that the crystallinity of **1** was maintained after a long-term photocatalytic process. The SEM image reveals no obvious changes in morphology, and a homogenous distribution of C, Cd, Cl, and N atoms was detected from the elemental mapping images (Fig. S20†). Besides, these elements could also be detected by the XPS spectrum. The high-resolution XPS spectra indicate the presence of the Cd^{2+} $2p_3$ and Cd^{2+} $2p_1$ spin orbitals from the main binding energy peaks at 406.1 and 412.8 eV, respectively (Fig. S21†).

Encouraged by its accessible synthesis, high physicochemical stability and outstanding photophysical performance, green and white LED devices were fabricated by coating **1** alone or a mixture of **1** and commercial red phosphor N630 (w/w: 3 : 1) on a commercial 365- or 460-nm diode chip, respectively, and then dried at 100 °C. Fig. 7a depicts the PL spectra of green LED devices under different drive currents (20–180 mA). It can be observed that the PL emission peak of the green LED device gradually enhances with the increase in drive currents without a change in the emission color. Photographs of the green LED device intuitively show that the emission light becomes brighter (Fig. 7b). Meanwhile, there is a good linear relationship between the maximum emission intensity and drive current, which can be fitted as a function $y = 0.68 + 0.92x$ with a correlation coefficient (R^2) of 0.998 (Fig. 7c). Detected by a thermal imager, the operating temperature of the green LED device can be up to 161 °C at a drive current of 180 mA (Fig. 7d), suggesting that **1** can be used to high-power green LED. Fig. 7e shows PL spectra of the white LED device fabricated with green phosphor of **1** and commercial red phosphor N630 on a 460 nm chip under various drive currents. Its emission intensity also exhibits a gradual increasing trend. At a drive current of 180 mA, the LED device generates white light with the CIE coordinate of (0.331, 0.334), correlated color temperature (CCT) of 6821 K, and color rendering index of 81.1. Therefore, the bright green [$CdCl_2$(AD)] phosphor can be considered as a promising green and white LED.

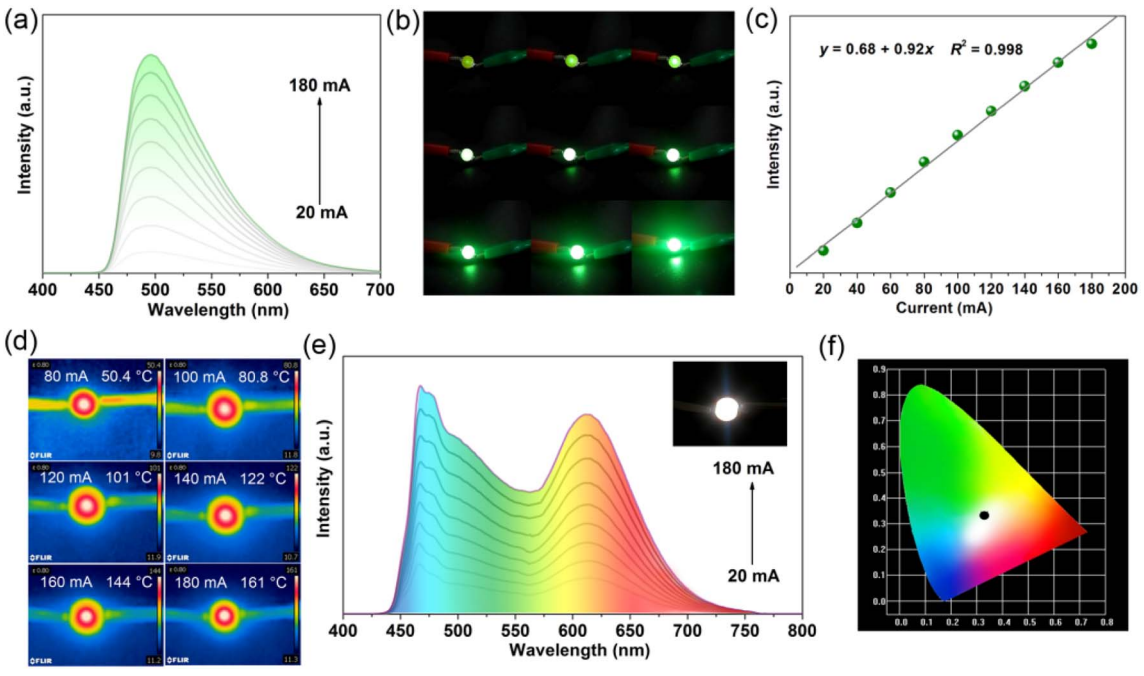

Fig. 7 PL spectra (a) and photographs (b) of [$CdCl_2$(AD)] based-green LED device with a 365 nm chip under various drive currents. (c) Relationship between the maximum emission intensity and drive currents of the green LED device. (d) Thermal images of the green LED device under various drive currents. (e) PL spectra of the white LED device fabricated with green phosphor [$CdCl_2$(AD)] and commercial red phosphor N630 on a 460 nm chip under various drive currents. (f) CIE-1931 chromaticity diagram of the white LED device under 180 mA drive current.

Conclusions

In summary, one new MOF phosphor [$CdCl_2$(AD)] (**1**) has been synthesized successfully under facile solvothermal conditions. In this MOF, the bulk π-conjugated AD photoactive molecules are tightly anchored by the $CdCl_2$ inorganic chain through strong coordination bonds and π···π stacking interactions between the AD molecules. Meanwhile, the $CdCl_2$ inorganic chains were surrounded by AD organic components, affording a dense stacking structure with high rigidity. Such structural characteristics substantially minimize the emission loss with increasing temperature and efficiently prevent the MOF from thermal quenching and ingression of water molecules. In addition, the alternating arrangement of the delocalized organic π-conjugated channels and $CdCl_2$ inorganic chains facilitates charge transfer, enabling the MOF's high emission efficiency and photoelectric performance. The accessible synthesis, outstanding optical performance, and low thermal quenching enable this MOF to work as a promising phosphor for green and white LED devices. Therefore, the findings of this research provide new ideas for designing MOF-based phosphors with a low thermal quenching character for potential solid-state lighting.

Data availability

The data supporting this article have been included as part of the ESI.† Crystallographic data for [$CdCl_2$(AD)] (CCDC No. 2364270) can be acquired free of charge from the Cambridge Crystallographic Date Centre *via* **http://www.ccdc.cam.ac.uk/conts/retrieving.html**.

Author contributions

Y.-J. Chen, P.-P. Yin, Y. Li, S.-Y. Yang, and Y.-M. Li synthesized and characterized the MOF. X.-G. Yang determined the single-crystal structure and performed the theoretical calculations and LED devices. X.-G. Yang, and Y.-J. Chen, wrote the manuscript. X.-G. Yang, and L.-F. Ma designed and directed the studies. All the authors discussed the results and reviewed the manuscript.

Conflicts of interest

There are no conflicts to declare.

Acknowledgements

This work was supported by the National Natural Science Foundation of China (No. 22371109, 22171123, 21971100), the Science Fund for Distinguished Young Scholars in Henan Province (No. 242300421036) and the Project for Science & Technology Innovation Talents in Universities of Henan Province (No. 21HASTIT006).

Notes and references

1 S. Tonzani, *Nature*, 2009, **459**, 312–314.
2 (*a*) A. Karmakara and J. Li, *Chem. Commun.*, 2022, **58**, 10768–10788; (*b*) X. Lv, R. Xiao, J. Liu, C. Yang, Y. Xina and N. Guo, *Inorg. Chem. Front.*, 2024, **11**, 1668–1682.
3 (*a*) K. Panigrahi and A. Nag, *J. Phys. Chem. C*, 2022, **126**, 8553–8564; (*b*) J. Hu, R. V. Deun, P. F. Smet and D. V. Heggen, *Mater. Adv.*, 2024, **5**, 231–239.
4 Y. Huang, W. Feng, Z. Zhou, H. Zheng, Y. Zhao, H. Yan and X. Lü, *J. Mater. Chem. C*, 2022, **10**, 7586–7593.
5 L. Kang and Z. Lin, *Inorg. Chem. Front.*, 2023, **10**, 13–36.
6 R. Sun, D. Zhou, Y. Ding, Y. Wang, Y. Wang, X. Zhuang, S. Liu, N. Ding, T. Wang, W. Xu and H. Song, *Light: Sci. Appl.*, 2022, **11**, 340.
7 H. Ding, J. Li, G. Xie, G. Lin, R. Chen, Z. Peng, C. Yang, B. Wang, J. Sun and C. Wang, *Nat. Commun.*, 2018, **9**, 5234.
8 L. Chen, C.-C. Lin, C.-W. Yeh and R.-S. Liu, *Materials*, 2010, **3**, 2172–2195.
9 S. Liu, X. Fang, B. Lu and D. Yan, *Nat. Commun.*, 2020, **11**, 4649.
10 A. Espasa, M. Lang, C. F. Aguiño, D. Sanchez-deAlcazar, J. P. Fernández-Blázquez, U. Sonnewald, A. L. Cortajarena, P. B. Coto and R. D. Costa, *Nat. Commun.*, 2020, **11**, 879.
11 O. M. Kate, J. R. Ommen and H. T. Hintzen, *J. Mater. Chem. C*, 2019, **7**, 6289–6300.
12 (*a*) J. Tian and W. Zhuang, *Inorg. Chem. Front.*, 2021, **8**, 4933–4954; (*b*) X. Lu, K. Zhang, X. Niu, D.-D. Ren, Z. Zhou, L.-L. Dang, H.-R. Fu, C. Tan, L.-F. Ma and S.-Q. Zang, *Chem. Soc. Rev.*, 2024, **53**, 6694–6734; (*c*) J. Li, C. Wang, Y. Niu, Y. Wang, F. Wu, Q. Zhang, Y. Teng, H. Dong and Z. Mu, *Ceram. Int.*, 2024, **50**, 18647–18654.
13 Y. H. Kim, P. Arunkumar, B. Y. Kim, S. Unithrattil, E. Kim, S.-H. Moon, J. Y. Hyun, K. H. Kim, D. Lee, J.-S. Lee and W. B. Im, *Nat. Mater.*, 2017, **16**, 543–550.
14 Q. Ma, N. Guo, Y. Xin and B. Shao, *Inorg. Chem. Front.*, 2021, **8**, 4072–4085.
15 M. L. Ding, R. W. Flaig, H. L. Jiang and O. M. Yaghi, *Chem. Soc. Rev.*, 2019, **48**, 2783–2828.
16 S. N. Sun, N. Li, J. Liu, W. X. Ji, L. Z. Dong, Y. R. Wang and Y. Q. Lan, *Natl. Sci. Rev.*, 2021, **8**, nwaa195.
17 Y. F. Zhao, H. Zeng, X.-W. Zhu, W. G. Lu and D. Li, *Chem. Soc. Rev.*, 2021, **50**, 4484–4513.
18 X. G. Yang, J. R. Zhang, X. K. Tian, J. H. Qin, X. Y. Zhang and L. F. Ma, *Angew. Chem., Int. Ed.*, 2022, **62**, e202216699.
19 E. M. Johnson, S. Ilic and A. J. Morris, *ACS Cent. Sci.*, 2021, **7**, 445–453.
20 P. Chen, J. S. Sun, L. Zhang, W. Y. Ma, F. Sun and G. Zhu, *Sci. China Mater.*, 2019, **62**, 194–202.
21 (*a*) X. G. Yang, X. M. Lu, Z. M. Zhai, Y. Zhao, X. Y. Liu, L. F. Ma and S. Q. Zang, *Chem. Commun.*, 2019, **55**, 11099–11102; (*b*) S. Zheng, Y. Ru, H. Xue and H. Pang, *Chin. Chem. Lett.*, 2021, **32**, 3817–3820.
22 (*a*) P. Mialane, C. M. Draznieks, P. Gairola, M. Duguet, Y. Benseghir, O. Oms and A. Dolbecq, *Chem. Soc. Rev.*, 2021, **50**, 6152–6220; (*b*) A. Chauhan and R. Langyan, *Rare*

Met., 2021, **40**, 2618–2626; (*c*) G. Si, X. Kong, T. He, W. Wu, L. Xie and J. Li, *Chin. Chem. Lett.*, 2021, **32**, 918–922; (*d*) H. R. Fu, R. Y. Zhang, D. D. Ren, K. Zhang, J. Yuan, X. Y. Lu and Q. R. Ding, *Cryst. Growth Des.*, 2024, **24**, 4819–4824.

23 (*a*) J. Tang, S. B. Zheng, S. X. Jiang, J. Li, T. Guo and J. H. Guo, *Rare Met.*, 2021, **40**, 478–488; (*b*) H. R. Fu, D. D. Ren, K. Zhang, H. Chen, X. Lu, Q. R. Ding and L. F. Ma, *Chin. J. Chem.*, 2024, **42**, 1260–1266; (*c*) H. R. Fu, D. D. Ren, K. Zhang, R. Y. Zhang, X. Y. Lu, Y. P. Wu, F. Aznarez, Q. R. Ding, L. F. Ma and D. S. Li, *ACS Mater. Lett.*, 2024, **6**, 2559–2568.

24 Y. Cui, J. Zhang, H. He and G. Qian, *Chem. Soc. Rev.*, 2018, **47**, 5740–5785.

25 X.-Y. Liu, W. P. Lustig and J. Li, *ACS Energy Lett.*, 2020, **5**, 2671–2680.

26 H. E. Emam, M. El-Shahat and R. M. Abdelhameed, *J. Hazard. Mater.*, 2021, **414**, 125509.

27 R. M. Abdelhameed, A. A. Shaltout, M. H. H. Mahmoud and H. E. Emam, *Sustainable Mater. Technol.*, 2021, **29**, e00326.

28 R. M. Abdelhameed, M. Taha, H. Abdel-Gawad and H. E. Emam, *J. Mol. Struct.*, 2022, **1250**, 131914.

29 A. Sharma, D. Kim, J. H. Park, S. Rakshit, J. Seong, G. H. Jeong, O. H. Kwon and M. S. Lah, *Commun. Chem.*, 2019, **2**, 39.

30 X. G. Yang, Z. M. Zhai, X. M. Lu, J. H. Qin, F. F. Li and L. F. Ma, *Inorg. Chem.*, 2020, **59**, 10395–10399.

31 X. M. Kang, H. S. Hu, Z. L. Wu, J. Q. Wang, P. Cheng, J. Li and B. Zhao, *Angew. Chem., Int. Ed.*, 2019, **131**, 16763–16769.

32 G. S. Alba, G. M. Miguel, B. Mariam, J. V. G. Ignacio, L. Marta, G. Felipe and A. D. L. P. O. Víctor, *J. Am. Chem. Soc.*, 2020, **142**, 318–326.

33 X. G. Yang, Z. M. Zhai, X. M. Lu, L. F. Ma and D. Yan, *ACS Cent. Sci.*, 2020, **6**, 1169–1178.

34 X. G. Yang, L. F. Ma and D. Yan, *Chem. Sci.*, 2019, **10**, 4567–4572.

35 (*a*) M. Z. Li and Z. G. Xia, *Chem. Soc. Rev.*, 2021, **50**, 2626–2662; (*b*) C. Xing, B. Zhou, D. Yan and W.-H. Fang, *Adv. Sci.*, 2024, **11**, 2310262.

36 (*a*) H. Y. Dong, C. H. Zhang, X. L. Liu, J. N. Yao and Y. S. Zhao, *Chem. Soc. Rev.*, 2020, **49**, 951–982; (*b*) C. Xing, B. Zhou, D. Yan and W.-H. Fang, *CCS Chem.*, 2023, **5**, 2866–2876; (*c*) J. Heine, B. Peerless, S. Dehnen and C. Lichtenberg, *Angew. Chem., Int. Ed.*, 2023, **62**, e2022187; (*d*) C. Xing, Z. Qi, B. Zhou, D. Yan and W.-H. Fang, *Angew. Chem., Int. Ed.*, 2024, **63**, e202402634.

37 (*a*) G. Xiao, Y.-J. Ma, Z. Qi, X. Fang, T. Chen and D. Yan, *Chem. Sci.*, 2024, **15**, 3625–3632; (*b*) Q. Liu, S. Gao, L. Xu, W. J. Yue, C. W. Zhang, H. Kan, Y. Li and G. Z. Shen, *Chem. Soc. Rev.*, 2022, **51**, 3341–3379; (*c*) B. Zhou and D. Yan, *Matter*, 2023, **6**, 3126–3129.

38 R. Chen, W. Zhou, Y. Gong, Z. Zhou, H. Wang, C. Dai, Y. Zhao, Y. Che, C. Zhang and J. Yao, *J. Mater. Chem. C*, 2022, **10**, 9945–9952.

39 Z. X. Lu, S. J. Wang, G.-L. Li, Z. Zhuo, H. M. Zhu, W. Wang, Y.-G. Huang and M. C. Hong, *ACS Appl. Mater. Interfaces*, 2022, **33**, 37894–37903.

40 V. Rajendran, M.-H. Fang, W.-T. Huang, N. Majewska, T. Lesniewski, S. Mahlik, G. Leniec, S. M. Kaczmarek, W. K. Pang, V. K. Peterson, K. M. Lu, H. Chang and R. S. Liu, *J. Am. Chem. Soc.*, 2021, **143**, 19058–19066.

41 J. J. Feng, H. M. Liu, Z. Ma, J. H. Feng, L. F. Chen, J. H. Li, Q. G. Zeng, D. W. Wen and Y. Guo, *Chem. Eng. J.*, 2022, **449**, 137892.

42 D. W. Wen, H. M. Liu, Y. Guo, Q. G. Zeng, M. M. Wu and R. S. Liu, *Angew. Chem., Int. Ed.*, 2022, **61**, e202204411.

43 J. W. Qiao, G. J. Zhou, Y. Y. Zhou, Q. Y. Zhang and Z. G. Xia, *Nat. Commun.*, 2019, **10**, 5267.

44 M.-H. Fang, P.-Y. Huang, Z. Bao, N. Majewska, T. Lesniewski, S. Mahlik, M. Grinberg, G. Leniec, S. M. Kaczmarek, C. W. Yang, K.-M. Lu, H.-S. Sheu and R.-S. Liu, *Chem. Mater.*, 2020, **32**, 2166–2171.

45 S. Wu, P. X. Xiong, Q. Liu, Y. Xiao, Y. S. Sun, E. H. Song and Y. Chen, *Adv. Opt. Mater.*, 2022, **23**, 2201718.